Transient Photoconductivity in Vitreous As_2Se_3

M. E. SCHARFE
Xerox Corporation, Rochester, New York 14604
(Received 24 June 1970)

This paper reports the study of the photogeneration and charge transport of holes in evaporated samples of vitreous As_2Se_3. The photogeneration is characterized by a field-dependent quantum efficiency which is similar to that found in vitreous Se. The charge transport is described by assuming a distribution of mobilities each of which has the same field dependence. The largest mobility of the distribution is approximately 4×10^{-5} cm^2/V sec at a field of 10^5 V/cm. The value of the largest mobility varies somewhat from sample to sample, but all samples exhibit the same functional form for the field dependence ($\mu \propto E$). The effects of preexposure with bulk absorbed light are demonstrated in order to emphasize the importance of performing these measurements on dark-rested samples. The electroded transient photoconductivity measurements are correlated with xerographic measurements to show a consistency between the different measurement techniques.

Recently, there has been an appreciable amount of interest in electronic transport through disordered photoconductor systems. In particular, the chalcogenide glasses have received considerable attention because they exhibit properties which make them useful in practical photoconductor devices including xerographic imaging systems and vidicon tubes. The chalcogenide glasses also exhibit interesting nonphotoconductive effects such as those associated with the recently reported switching and memory devices.[1]

The best-known chalcogenide glass is vitreous Se. The photogeneration and electronic transport properties of this material have been well characterized. The photogeneration was found to be field dependent[2,3] and the transport of both the holes and electrons was found to be governed by a trap-controlled drift mobility.[4,5] As an extension of the work on Se, Tabak considered the As-Se alloy system (0–40% As) and correlated changes in the hole and electron transport with As concentration to changes in the structural components of the alloy.[6] In that study, it was observed that for As concentrations greater than 5% by weight the photoinduced discharge voltage for hole transport could no longer be characterized by a simple transit time model as in the vitreous Se case. Instead the discharge was characterized by a time-resolved "discharge tail" from which a mobility of 10^{-5} cm^2/V sec was estimated.[6] Viscakas *et al.* have described similar effects.[7] Kolomiets and Lebedev also noted this type of behavior in As-Se alloys and estimated a mobility of 4×10^{-4} cm^2/V sec from transport measurements using electron beam excitation.[8]

The purpose of this paper is to characterize the photogeneration and transport properties of holes in vitreous As_2Se_3. This system was chosen since it represents a stoichiometric combination of these materials as they are combined in the crystalline phase. This alloy also exhibits the slow discharge tail characteristic of the As-Se alloys but does not show the initial "fast" response as seen in alloys with smaller As concentrations (<18% As).[6,9] It will be shown that the photogeneration of carriers is field dependent, as in vitreous Se, and that the transport in the photoinduced discharge can be described by assuming a distribution of "effective mobilities." The largest mobility and the average mobility of this distribution can be measured directly from the discharge curves. In addition, it will be shown that these mobilities are *electric field dependent*, varying linearly with the applied field. Finally, the effects of preexposure with bulk absorbed light will be demonstrated in order to emphasize the importance of resting procedures in these measurements.

The results were obtained using two measurement techniques. One was a time-resolved transient photoconductivity measurement which employed a sandwich cell sample structure to measure the photoinduced discharge current.[6,10] This current was monitored as a function of applied bias voltage, excitation wavelength, excitation intensity, and sample thickness. The other technique consisted of xerographic discharge measurements which were made under continuous illumination with a corona-charged surface.[11] The transient measurements are correlated with the xerographic measurements to show a consistency between the different techniques, especially in terms of comparing the field-dependent photogeneration property of the material.

THEORY

The theoretical considerations necessary for a description of the experimental results are divided into three parts. The first part includes a derivation of the transient photoinduced discharge current, under small signal conditions, assuming a distribution of field-dependent mobilities. The second part consists of a formulation of the large signal (space-charge limited) case for the same mobility distribution. Finally, the third part deals with the xerographic discharge under continuous illumination.

Small-Signal Case

The transient photoinduced discharge for the small-signal case has been discussed in detail by several

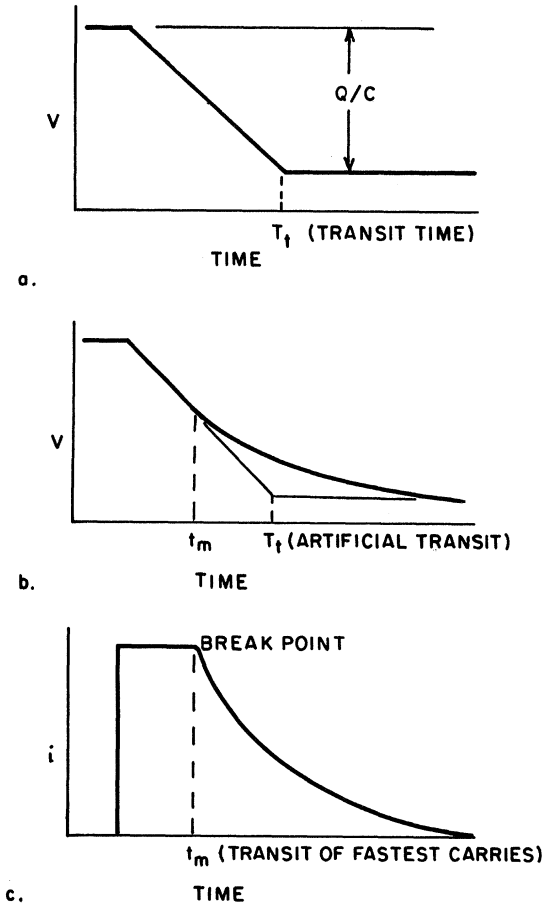

FIG. 1. Typical transient photoinduced discharges: (a) the discharge voltage across a material with a unique mobility, (b) the discharge voltage across a material with a distribution of mobilities, and (c) the discharge current through a material with a distribution of mobilities.

authors.[2,4,5] In these discussions, the discharge is described in terms of a sheet of charge drifting through the bulk of the material with a velocity equal to μE, where μ is the carrier drift mobility and E the magnitude of the applied electric field. When applied to an insulating photoconductor with a uniform trap density and no unneutralized bulk space charge, this analysis gives the following equation for the voltage discharge across the sample:

$$v(t)=[Q(E)\mu E\tau/CL][1-\exp(-t/\tau)], \quad t\leq T_t. \tag{1}$$

In Eq. (1), $Q(E)$ is the photogenerated charge, τ the free-carrier lifetime as determined by capture by deep traps, T_t the transit time ($T_t=L/\mu E$), L the sample thickness, and C the effective capacity of the sample (including any stray external capacitance). This equation applies only to cases where the duration of the light pulse is much shorter than the transit time T_t.

If the ratio of T_t to τ becomes small, implying little trapping before T_t, Eq. (1) reduces to

$$v(t)=Q(E)\mu Et/CL, \quad t\leq T_t \tag{2}$$

and

$$v(T_t)=Q(E)\mu ET_t/CL=Q(E)/C, \quad t\geq T_t. \tag{3}$$

For this special case ($\tau\gg T_t$), the voltage discharge is a linear ramp function for times less than the transit time and then saturates at a value of $Q(E)/C$ when all the carriers have drifted across the material [see Fig. 1(a)].

Only in a few instances are clearly defined ramp-type transits observed in photoinduced discharge measurements. Pulse shapes are generally rounded indicating dispersive effects, e.g., diffusion during the drift or carriers moving with different effective mobilities. We choose to represent these effects by assuming a distribution of drift mobilities. In this model the injected charge does not drift as a well-defined sheet but disperses as it drifts owing to the variation in the effective transit times. Physically, the dispersion can be attributed to a distribution of release times in the context of a shallow trap controlled drift mobility. This implies nonequilibrium between the trapping states and transport states over the time duration of the transport. The time-dependent discharge can then be divided into two components. At a given time, one component represents the voltage discharge due to all charge which is in transit and has not reached the back electrode. The other component represents the discharge due to the charge which has completed the transit across the material and has been collected. The sum of these terms represents the total discharge at any time t_j, as is given by

$$v(t)=\frac{Q(E)Et_j}{CL}\int_0^{\mu_j}\mu' P(\mu')d\mu' + \frac{Q(E)}{C}\int_{\mu_j}^{\infty}\left(P(\mu')d\mu' \Big/ \int_0^{\infty}P(\mu')d\mu'\right), \tag{4}$$

where $P(\mu')$ represents the probability that the mobility is between μ' and $\mu'+d\mu'$, and μ_j represents the mobility of the fastest carrier still in transit. This is represented schematically in Fig. 2(a). The distribution is normalized so that

$$\int_0^{\infty}P(\mu')d\mu'=1 \quad \text{and} \quad \mu_j=L/Et_j.$$

In this formulation all deep-trapping effects have been neglected and the excitation light pulse is assumed to be much shorter than the transit time of the fastest carriers. If the mobility were unique, we see that the first part of Eq. (4) would reduce to Eq. (2) and the second part would equal Eq. (3).

In order to obtain a better understanding of the kinetics of the discharge, consider a mobility distribution $P(\mu)$ as shown in Fig. 2(b). This represents a constant, normalized distribution with mobilities varying from zero to μ_m. If we consider times less than $L/E\mu_m$ which means that no carriers have reached the

back electrode, then $v(t)$ is given by

$$v(t)=\frac{Q(E)Et_j}{CL}\int_0^{\mu_m}\mu'(\mu_m)^{-1}d\mu'$$
$$=Q(E)E\mu_m t_j/2L, \quad t_j<L/E\mu_m. \qquad (5)$$

By comparing Eq. (5) to Eq. (2), it is seen that the discharge can be described as a linear ramp function with an "effective" mobility $\frac{1}{2}\mu_m$. This means that until the first carrier has reached the back electrode, there is no functional difference between the two cases. This is not unique for the distribution in this example but is true for any distribution $P(\mu)$ which has an upper limit on the mobility. If now we consider times t_j where $t_j>L/E\mu_m$, Eq. (4) becomes

$$v(t)=\frac{Q(E)Et_j}{CL}\int_0^{\mu_j}\mu'(\mu_m)^{-1}d\mu'$$
$$+\frac{Q(E)}{C}\int_{\mu_j}^{\mu_m}(\mu_m)^{-1}d\mu', \quad \mu_j=L/Et_j. \qquad (6)$$

Performing the integrations, we obtain

$$v(t)=[Q(E)/C](1-L/2Et_j\mu_m), \quad t_j>L/E\mu_m. \qquad (7)$$

Figure 1(b) represents the total transient voltage discharge curve as a function of time obtained from the $P(\mu)$ distribution shown in Fig. 2(b). The discharge for $t>t_m$ [Eq. (7)] is the "discharge tail" which is characteristic of the As-Se photoconductor system.[6]

If an arbitrary discharge is analyzed by usual transient photoconductivity measurement techniques, erroneous interpretations can result. For example, transit times have generally been obtained by measuring the time where the asymptote to the initial discharge intersects with the final pulse height as demonstrated in Fig. 1(b). In the case of a well-defined mobility as in vitreous Se at room temperature, this technique is effective and measures the transit time of the carriers. However, if there is significant dispersion, this interpretation yields an *artificial* transit time which does not represent the real kinetics of the discharge. Secondly, it is usually difficult to measure the total discharge pulse height in very-low-mobility materials owing to time-constant limitations of the experimental circuitry. For example, the $P(\mu)$ distribution shown in Fig. 2(b) would require a circuit with an infinite time constant in order to measure the saturated pulse height, since the mobility distribution extends to zero.

A much better method of observing the transport processes is to measure the transient photoinduced discharge current instead of the voltage. This current, which is equal to $C\,dv(t)/dt$, amplifies functional changes in $v(t)$ which are associated with the transport. If we take the derivative of the curve in Fig. 1(b), the photoinduced discharge current is constant until the first carriers transit across the sample at time $t_m=L/E\mu_m$. This is shown schematically in Fig. 1(c). After t_m, the current decreases as a function of time with the

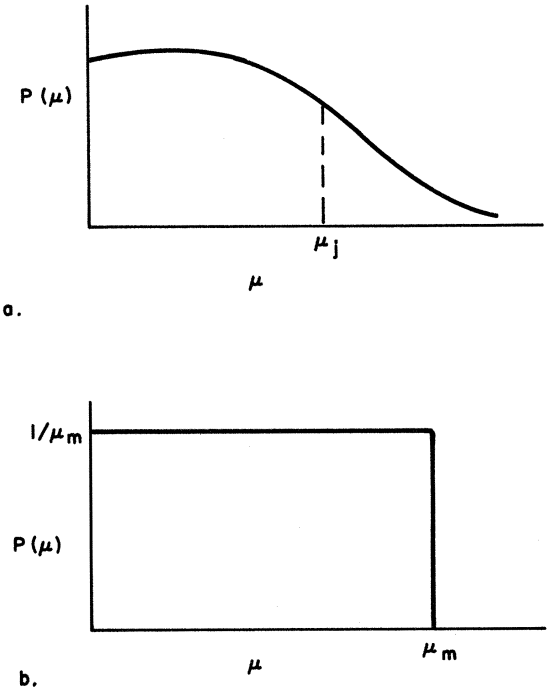

FIG. 2. (a) Arbitrary distribution of mobilities in a photoconducting material. (b) Normalized distribution of mobilities for a material with mobilities varying from zero to μ_m. $P(\mu')$ represents the probability that the mobility is between μ' and $\mu'+d\mu'$.

functional form depending on the mobility distribution $P(\mu)$. Therefore, from the current mode discharge, we can obtain the largest mobility from the "break point" in the discharge and the distribution of $P(\mu)$ from the transient decay after the break point. The field dependence of the fastest transit time and the mobility distribution is obtained by varying the applied bias field and observing the changes in the photoinduced discharge current.

The average value of $P(\mu)$ can be obtained from the magnitude of the current measured before t_m. This current is given by

$$i(t)=\frac{Q(E)E}{L}\int_0^{\mu_m}\mu'P(\mu')d\mu', \qquad t\leq t_m \qquad (8)$$

which is simply C multiplied by the derivative of the first term in Eq. (4). Since $P(\mu)$ is normalized, the integral

$$\int_0^{\mu_m}\mu'P(\mu')d\mu'$$

represents the average mobility. Therefore, Eq. (8) can be written as

$$i(t)=[Q(E)E/L]\mu_{\rm av}, \qquad t\leq t_m \qquad (9)$$

which means that if $Q(E)$ is known the average value of the mobility is determined. If the situation is further

complicated by a field-dependent mobility, the preceding equations can be modified to include this effect by substituting $\mu(E)$ for μ.

Large-Signal Case

The large-signal or transient space-charge-limited discharge for materials with a unique mobility has been treated in considerable detail.[12,13] For example, Many and Rakavy have considered the transient space-charge-limited discharge for the case where the surface field is driven to zero for all time.[12] This corresponds experimentally to situations where the discharge current is produced by an intense, continuous illumination. Their results indicated that under these conditions the measured transit time, t_1, becomes 20% smaller than that obtained for the space-charge-free case and the total transient trap-free discharge current can be represented by

$$J(t)=[\epsilon\mu V^2/2L^3](1-t/2T_t)^{-2} \quad \text{for} \quad 0\leq t\leq t_1. \quad (10)$$

Weisz *et al.* considered the case where the initial current was again space charge limited at $t=0$ as in Many and Rakavy's description but with the surface field driven to zero for times less than or equal to t_1.[14] This situation corresponds experimentally to pulsed-light photoconductivity measurements where the intensity of the light is large enough to drive the field to zero only for the pulse duration. In this work, as in Many and Rakavy's, the transient photoinduced discharge current was characterized by a rising function with an initial current of $\epsilon\mu V^2/2L^3$ and a cusp at the reduced transit time t_1. The actual functional form for $J(t)$, however, was different from that of Many and Rakavy's due to the different boundary conditions. In general, it is concluded that the reduced transit time t_1 is caused by the increasing field that the charge sheet feels as it drifts across the material and the rising current before the cusp is due to a combination of both the increasing field and the increasing injected charge determined by the duration of the light pulse.

If a distribution of mobilities is assumed, the transient space-charge-limited current results must be viewed somewhat differently. For example, if a mobility distribution as shown in Fig. 2(a) is considered, the voltage dependence of the space-charge-limited current (SCLC) at $t=0$ must be modified to include the average mobility of the distribution. This result is derived from the basic transport equations which require that the initial SCLC be given by

$$J_{\mathrm{SCLC}}(0)=Q_0 v_{\mathrm{av}}/L=\epsilon E v_{\mathrm{av}}/L, \quad (11)$$

where Q_0 represents the photogenerated charge per cm^2, which is equal to ϵE for SCLC conditions and v_{av} is the average velocity of the injected carriers. The average velocity is simply

$$v_{\mathrm{av}}=\int_0^E \mu_{\mathrm{av}} E'dE' \Big/ \int_0^E dE'=\tfrac{1}{2}\mu_{\mathrm{av}}E. \quad (12)$$

Substituting Eq. (12) into Eq. (11) and replacing E by V/L, $J_{\mathrm{SCLC}}(0)$ becomes

$$J_{\mathrm{SCLC}}(0)=\epsilon\mu_{\mathrm{av}}V^2/2L^3. \quad (13)$$

If the mobility, in addition to being dispersed, is also field dependent, the initial SCLC will be changed not only in magnitude but also functionally. This can be demonstrated by assumiug that the field dependence of the average mobility varies as a power function of the applied field. In this case, the SCLC at $t=0$ can be represented as

$$J_{\mathrm{SCLC}}(0)=\frac{\epsilon E}{L}\int_0^E \mu_{\mathrm{av}}\left(\frac{E'}{E_0}\right)^{\alpha} E'dE' \Big/ \int_0^E dE', \quad (14)$$

where α is a number representing the field dependence of the mobility and $E_0{}^{\alpha}$ is the normalizing factor. Performing the integration in Eq. (14) and substituting V/L for E, the current becomes

$$J_{\mathrm{SCLC}}(0)=\epsilon\mu_{\mathrm{av}}V^{\alpha+2}/E_0{}^{\alpha}(\alpha+2)L^{\alpha+3}. \quad (15)$$

This predicts that the voltage dependence of $J(0)$ will always be larger than that for the field-independent case.

Xerographic Case

The xerographic measurements are considerably different from the transient studies described above. In the xerographic case, *no* electrodes (except for the substrate) are placed on the material and the bias is applied by a high-voltage corona discharge which sprays charge onto the photoconductor surface. The experiment is performed by charging the material to a

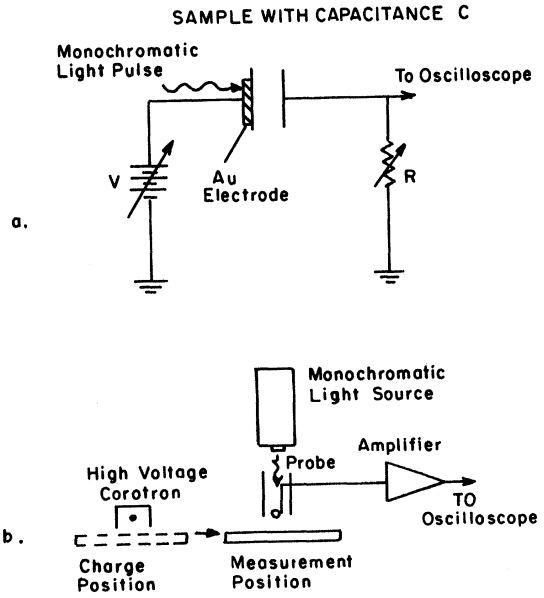

FIG. 3. (a) Schematic diagram of the experimental circuitry used for the transient photoconductivity measurements. (b) The experimental configuration used to perform the xerographic measurements.

known field and subsequently discharging the photoconductor by exposure to a continuous light source. Under these conditions, the measurement time is much longer than the transit time of the carriers, which means that the discharge current can be represented as

$$i(t, E)=G(E)eF\approx C\Delta v(t)/\Delta t_{t=0^+}$$
$$\text{for } \Delta v(t)\ll V \text{ and } \Delta t\gg T_t. \quad (16)$$

In this equation $G(E)$ is the quantum efficiency, e the electronic charge, F the photon flux, T_t the transit time of the slowest carriers, and V the surface potential of the photoconductor. The condition $t=0^+$ implies that $\Delta v(t)/\Delta t$ is taken at the time when the exposure is applied and the E term is simply V/L. This equation implies that $\Delta v(t)/\Delta t_{t=0^+}$ is proportional to the quantum efficiency $G(E)$. Therefore, by plotting $\Delta v(t)\Delta t_{t=0^+}$ versus E or V, we can obtain the functional form of the field-dependent photogeneration property of the material. This, only holds true when there is no bulk trapping.

A correlation between the xerographic results and the transient results can be made by comparing the field-dependent quantum efficiency measurements for each case. As shown above, the quantum efficiency is directly proportional to $\Delta v(t)/\Delta t_{t=0^+}$ for the xerographic case. The quantum efficiency for the transient case can be obtained from Eq. (9) by replacing $Q(E)$ with $G(E)eF'$ (where F' represents the total number of incident photons) and integrating both sides of the equation from $t=0$ to t_m. Performing these operations we find that

$$\int_0^{t_m} i(t)\,dt=G(E)eF'(E\mu_{av}t_m/L). \quad (17)$$

Since $t_m=L/\mu_m E$, Eq. (17) becomes

$$\int_0^{t_m} i(t)\,dt=G(E)eF'(\mu_{av}/\mu_m). \quad (18)$$

If the mobilities are field dependent and μ_{av} and μ_m have the same field dependence, then

$$\int_0^{t_m} i(t)\,dt\propto G(E).$$

EXPERIMENTAL TECHNIQUE

The samples were prepared by evaporating vitreous pellets of As_2Se_3 onto aluminum substrates kept between 200 and 225°C. After preparation, semitransparent Au or Al electrodes were deposited on each sample to provide electrical contact to the photoconductor. The samples were then mounted into a holder which provided adequate electrical shielding and easy access for experimentation.

The experimental circuitry is shown schematically in Fig. 3(a). This circuit is simply a series RC network with the capacitance C being the sample under investigation. The RC time constant was adjusted so that it was very short with respect to the transient discharge which was produced by a light flash of 5-μsec duration. Monochromatic light was obtained through the use of interference filters and the intensity was adjusted by neutral density filters. The experiment was completed by monitoring the time-resolved discharge current $[i(t)]$ which appeared as a transient discharge voltage across the resistor R. All measurements were performed at room temperature.

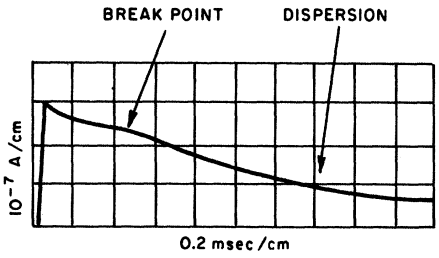

FIG. 4. Typical transient photoinduced discharge current trace for holes in vitreous As_2Se_3. A voltage of +700 V was applied to the illuminated electrode of a 41-μ sample. The exposure consisted of a 5-μsec 4000-Å light flash.

The experimental configuration for xerographic measurements is shown schematically in Fig. 3(b). The system is essentially a motor-driven table which enables the surface of the As_2Se_3 to be charged by a high-voltage corona discharge at one position and transports the As_2Se_3 to a second position where the photoinduced measurements are made. The discharge is produced by a shuttered Bausch and Lomb monochromatic light source. The discharge voltage is monitored by a thin wire probe which capacitively couples to the surface of the photoconductor and is transparent to the monochromatic light. The probe is electrically connected to a high-input impedance ($>10^{15}$ Ω) amplifier which measures the absolute magnitude of the photoinduced discharge as a function of time. The samples were dark-rested 15 min between each measurement.

RESULTS

Two types of transient photoinduced discharges are seen in vitreous As_2Se_3. These discharges are directly related to the semitransparent electrode material used in performing the measurements. With Au electrodes, the discharges show distinct transport effects which can be analyzed in terms of a distribution of field-dependent mobilities. The discharges for Al contacts do not show the same effects and cannot be analyzed in terms of the same mobility distribution. It is our opinion that polarization is responsible for the unusual discharges for Al electrodes. A discussion of these polarization effects will be delayed until after the results for samples with Au electrodes have been considered in detail and the transport properties of the material have been established.

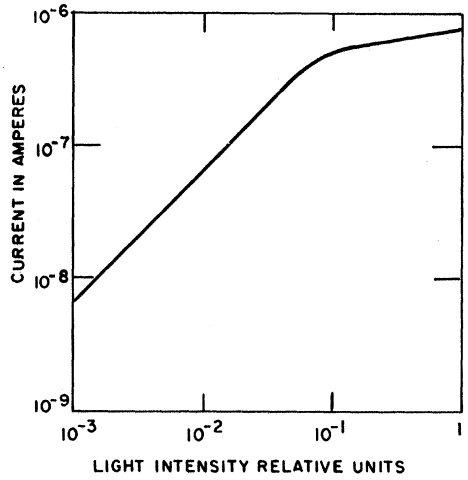

FIG. 5. Light-intensity dependence of the photoinduced discharge current for a 41-μ sample of vitreous As_2Se_3 biased at 10^5 V/cm. The exposure was produced by a 5-μsec 4000-Å light flash. The intensity was varied by neutral density filters.

Small- and Large-Signal Transients Results

A typical transient photoinduced discharge current trace for a sample with Au electrodes is shown in Fig. 4. From this trace, we can define the important properties of the photoinduced discharge which will be discussed in this paper. The transient current pulse height is defined as the magnitude of the current at the break point of the discharge trace. The initial current spike, shown in the figure at $t=0$, cannot be resolved in terms of its absolute magnitude due to time-constant limitations associated with the experimental circuitry. A discussion of the possible causes of this current spike will be considered in a later section. The transit time of the *fastest* carriers is taken as the time of the break point in the discharge current. The decaying discharge after the break point is defined as the dispersion in the photoinduced discharge and will be associated with a distribution of carrier mobilities.

Light-Intensity Dependence

With the preceding definitions in mind, the light-intensity dependence of the discharge-current pulse height for a 41-μ sample of vitreous As_2Se_2 is shown in Fig. 5. The current is seen to be linear over the lower 1.5 decades of light intensity and "saturates" to a 0.2 power dependence for very high light levels. The current trace for the highest light level with a 700-V bias is shown in Fig. 6. The discharge for the same sample under identical bias conditions but for a light intensity two orders of magnitude smaller is shown in Fig. 4. Comparing the curves, it is seen that only the magnitude of the current has changed significantly with intensity and not the functional form.

The amount of charge injected for the large signal case is close to the magnitude of the total surface charge (CV) on the sample. This is demonstrated by graphically integrating under the curve in Fig. 6. The transient discharge after the break point is approximately exponential with a time constant of 1.3×10^{-3} sec. Integrating this exponential from zero to infinity and adding the integral of the current up to the break point gives the total photoinjected charge of 10^{-8} C. The total surface charge (CV) is 1.6×10^{-8}C, where ϵ was assumed as 9 and the area of the electrode was 0.12 cm^2. The area beneath the initial spike of current was not included in the calculation nor was the "dark current" flow (all current flow not produced by the flash). Both of these factors would tend to increase the net amount of injected charge. This calculation shows that the current is at least space charge perturbed and close to space charge limited for the high light-intensity measurements.

Voltage and Wavelength Dependence

The voltage dependence of the transient photoinduced discharge current for both the small- and large-signal cases is shown in Fig. 7. Two orders of magnitude in light intensity separate the respective curves. As shown, the functional form of the curves changes considerably with intensity with the strongest voltage dependence for the highest light level.

The break point in the transient photoinduced discharge traces is associated with the transport of carriers through the bulk of the material. This is demonstrated by comparing the traces in Fig. 8 which show the effect of light absorption on the transient charge. The absorption constant for light with wavelengths between 4000 and 6500 Å [see Figs. 8(a)–8(c)] is greater than 10^4 cm^{-1}.[15] The light is therefore absorbed in distances small compared to the thickness of the sample. Consequently, the photogenerated charge is injected in a thin sheet which is necessary in order to observe the transport effects. As the excitation wavelengths approach 7000 Å [Fig. 8(d)], the shoulder and break point of the discharge disappear owing to the bulk absorption ($\alpha\approx10^3$ cm^{-1}) of the incident radiation.

The voltage dependence of the inverse transit time of the fastest carriers is shown in Fig. 9. The exposure and bias conditions are identical to those used for the

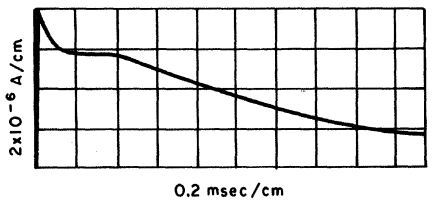

FIG. 6. Transient photoinduced discharge current trace for a 41-μ sample of vitreous As_2Se_3 for the highest light intensity available. The bias and exposure conditions are similar to those used in Fig. 4 except that the intensity is two orders of magnitude higher.

pulse-height measurements reported earlier. In some materials, i.e., vitreous Se at room temperature, a plot of $1/T_t$ versus V is linear with the slope of the curve equal to μ/L^2. For vitreous As_2Se_3, *the plot of $1/T_t$ versus V is not linear* as indicated in Fig. 9. *Consequently no unique mobility can be defined.* This implies that the carriers do not drift with a simple velocity of μE but drift as $\mu(E)E$, where $\mu(E)$ is arbitrarily defined as a field-dependent drift mobility. This definition is used as a means to discuss the shape of the $1/T_t$-versus-E curves and does not imply any physical significance to the transport processes. Under these assumptions $\mu(E)$ becomes (conforming to the notation used earlier)

$$\mu(E)=\mu_0(E^\alpha/E_0{}^\alpha)=\mu_0 E/E_0,$$

where E_0 is a normalizing factor and $\alpha=1$.

It is evident from Fig. 9 that light intensity does not change the effective transit time. As mentioned earlier, the 4000-Å exposure for the highest light intensity produced space-charge-perturbed conditions. The $1/T_t$ curve for this case is represented by dots in the figure. The $1/T_t$ curve for the same wavelength but for light intensities two orders of magnitude lower (unperturbed case) is represented by the circles. There are no significant differences in magnitude or functional form between these curves. The results of Weize *et al.* predict that the transit time will be reduced by approximately 20% under space-charge-perturbed conditions in materials with a unique field-independent mobility.[14] This effect is not present in vitreous As_2Se_3. It was also predicted that a current cusp would accompany the reduced transit time. This cusp is not seen in this material (similar effects are observed in *PVK*[16]). In a few samples, however, a very minor rise ($\approx$5 to 10%) in current did appear at the transit time. A discussion of these effects will be presented after the small-signal results have been considered in more detail.

The values for the mobility of the fastest holes in vitreous As_2Se_3 samples of different thicknesses are shown in Table I. All the mobilities were calculated

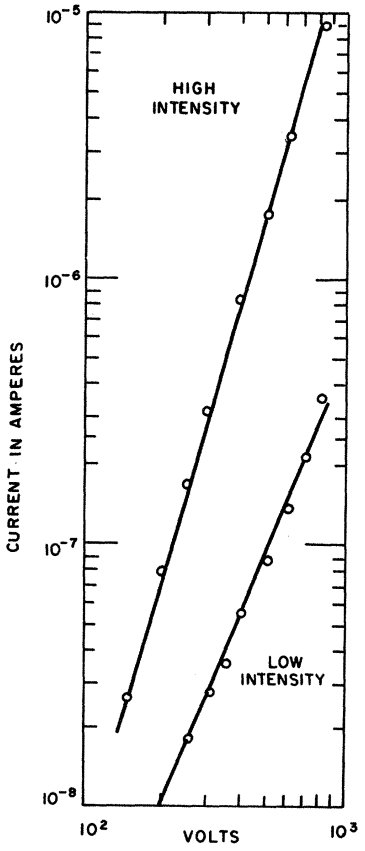

FIG. 7. Voltage dependence of the transient photoinduced discharge current for both small- and large-signal cases. The exposure was supplied by a 4000-Å 5-μsec light flash. Two orders of magnitude in light intensity separate the respective curves.

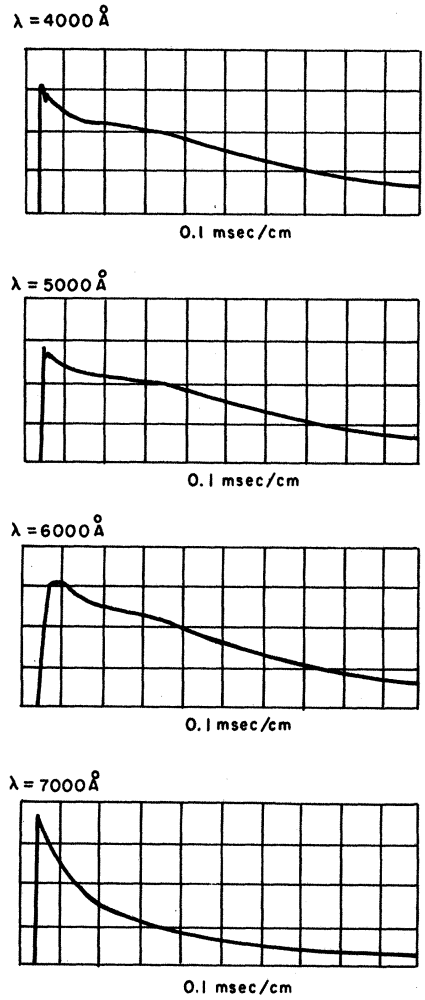

FIG. 8. Effect of wavelength (absorption) on the shape of the transient photoinduced discharge current. Each discharge is for a 30-μ sample of vitreous As_2Se_3 biased at 400 V. The light intensity was adjusted so that each wavelength gave approximately the same pulse height.

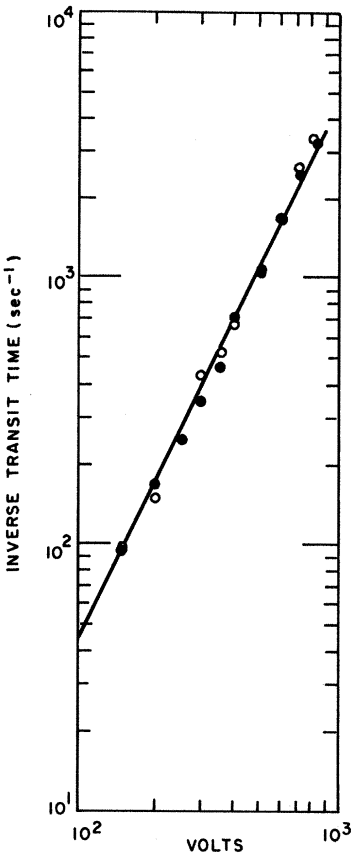

FIG. 9. Voltage dependence of the inverse transit time of the fastest carriers in a 41-μ sample of vitreous As_2Se_3. The exposure was supplied by 4000-Å 5-μsec light flash. The dots represent the transit times for a light intensity two orders of magnitude larger than the circles.

from the expression $\mu = L/T_t E$, where E was 10^5 V/cm and T_t was the transit time at that field. As shown, there is no relationship between the mobilities and the sample thicknesses. There is, however, considerable scatter in the magnitude of $\mu(E)$. Since $\mu(E)$ is not thickness dependent and the transit time changes with field, it is concluded that the break point is a real transport effect and the carriers are not range limited at these high fields. The discharge after T_t is assumed to be due to the drift of carriers with smaller mobilities. The functional form of the discharge is then determined by the specific $P(\mu)$ distribution.

With this model of the discharge in mind, we can use the I-versus-V and the $1/T_t$-versus-V results to obtain some further insight into the charge generation and transport. For example, the field dependence of the quantum efficiency can be obtained through Eq. (18). The integral

$$\int_0^{T_t} i(t)\,dt$$

is simply the product of $I(V)$ for the low-light-level case in Fig. 7 times $T_t(V)$ obtained from Fig. 9. This gives $G(V) \propto V^{0.5}$ or $E^{0.5}$, which is similar to the field-dependent quantum efficiency found in vitreous Se at comparable fields.[2,3] Secondly, the average mobility of the distribution can be obtained from Eq. (9) by substituting for $i(t)$ and $Q(E)$. Performing this substitution for the discharge in Fig. 4, we find that $\mu_{av} \approx 4.3 \times 10^{-5}$ cm^2/V sec (at 1.7×10^5 V/cm), where $Q(E)$ was obtained by graphically integrating the current. It was not possible to integrate the current directly owing to time-constant limitations.

Large-Signal Case

The large-signal space-charge-perturbed results for vitreous As_2Se_3 must be analyzed in a manner different from that used for materials with unique mobilities. In unique mobility materials, the large-signal phenomena (reduced transit and cusp) are produced by the increasing electric field felt by the carriers as they transit through the material. In vitreous As_2Se_3 this effect does not occur due to the large dispersion in transit times of the injected carriers. Because of this dispersion, most of the photogenerated charge is not displaced very far in times comparable to the transit time of the fastest carriers. Since not much charge is displaced, the internal field remains essentially constant during the transit. Consequently, the carriers see only the applied bias field of V/L and no cusps or reduced transit times are observed.

The voltage dependence of the large-signal space-charge-limited results can be obtained from Eq. (15). Since α equals 1 for vitreous As_2Se_3, the space-charge-limited current should vary as V^3. The measured large-signal currents shown in Fig. 7 vary as $V^{3.6}$. The discrepancy between the curves may be due to the inability to obtain a truly space-charge-limited current for all bias voltages. For example, if the ratio of photogenerated charge to total surface charge decreases with decreasing bias, the voltage dependence of the current will decrease faster than $V^{3.0}$. This effect can occur when the generation efficiency falls faster at the lower bias fields than at the higher fields and the light flash is not intense enough to sustain space-charge-limited con-

TABLE I. Measured mobilities for samples of different thicknesses at an applied electric field of 10^5 V/cm.

μ ($\times 10^{-5}$ cm^2/V sec)	L ($\times 10^{-4}$ cm)
4.0	4
5.0	14
4.75	28
7.5	30
3.2	41
1.73	76

ditions at these fields. It will be shown in the next section that the quantum efficiency falls faster than $E^{0.5}$ for fields less than 4×10^4 V/cm. Finally, the V^3 relation assumes no trapping which may not be true at very low bias voltages.

The initial current spike, which is present in all the discharges, could be causes by three unrelated effects. It could be due to the relaxation of the photoinjected charge into a distribution of localized states, a high-field region in the vicinity of the illuminated electrode, or it could be caused by electrons moving in the opposite direction. It was not possible to distinguish between these effects since the discharge for times near $t=0$ could not be measured due to RC time-constant limitations.

As mentioned earlier, samples with Al electrodes have different photoinduced discharges than those with Au electrodes. The photoinduced discharge for a sample with Al contacts is similar to that shown in Fig. 8(d). It is evident that there is no break point and consequently no unique transit time. One possible explanation is that it is caused by an internal negative space charge produced by trapping thermally generated electrons. The space charge modifies the field distribution which obscures all transport effects. This does not occur for Au contacts since holes are injected from the Au into the As_2Se_3 neutralizing the effects of polarization. This effect can be checked by exposing the Al electroded sample to a continuous light source to duplicate the injection effect. Under these conditions, the discharges for Al and Au contacts are similar. A second possible explanation for the different discharges could lie in the relaxation of injected charge into a distribution of localized states. In this case, the dark injected holes for samples with Au contacts could fill most of the deeper localized states before the light flash. Consequently, the photoinjected carriers would not interact with these states and the discharge would be modified. The difference, then, between the signals obtained for Al and Au is that in the case of Al electrodes the initial portion of the discharge is due primarily to the relaxation of the photogenerated carriers into the deeper states.

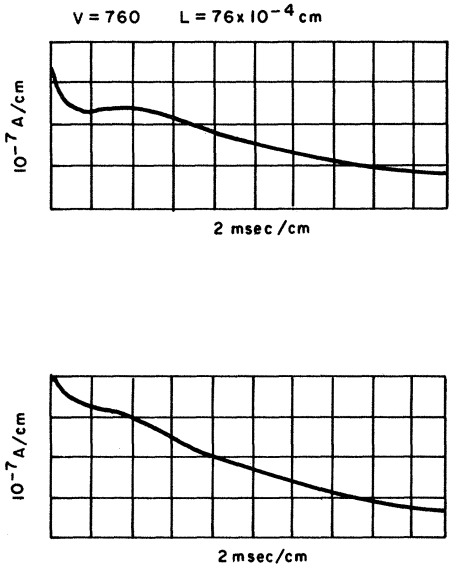

FIG. 10. Effects of red-light fatigue on the transient photoinduced discharge current in vitreous As_2Se_3. The upper part of the figure shows the unfatigued transient discharge. The lower part of the figure shows the same discharge after exposure to a tungsten light source.

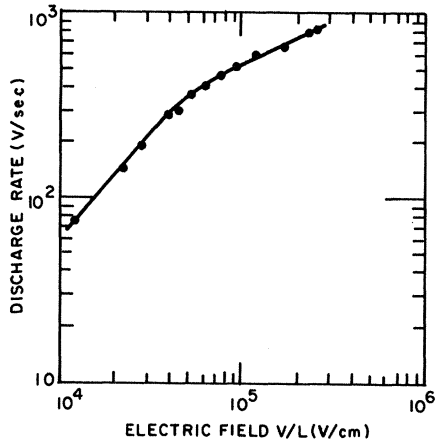

FIG. 11. Field dependence of the xerographic discharge rate for a 26-μ sample of vitreous As_2Se_3. The exposure was provided by 4000-Å illumination at an intensity of 2×10^{12} photons/cm² sec.

Fatigue Effects and Xerographic Results

The effects of red-light fatigue are demonstrated by the traces shown in Fig. 10. Light fatigue implies that the material was illuminated by a light source prior to applying the bias voltage. The dark-rested transient photoinduced discharge for a 76-μ sample exposed to 4000-Å radiation is shown in Fig. 10(a). The sample was then shorted and exposed to a tungsten source for several seconds to induce the fatigue effects. The subsequent discharge after the fatigue is shown in Fig. 10(b). It is clear that the fatigue has increased the photoinduced discharge, changed the shape of the discharge current, and reduced the effective transit time. These effects can be explained in terms of negative bulk space charge introduced by the tungsten exposure. Electrons are extremely range limited due to a very short trapping lifetime in vitreous As_2Se_3. The highly penetrating effects of the longer-wavelength radiation ($\geq$7000 Å) in the tungsten source produce hole-electron pairs in the bulk of the material.[6,7] The electrons are almost immediately trapped. Upon recharging the sample to the same voltage, the bulk space charge produced by the electrons enhances the electric field in the absorption region of the material. This means that the electric field is not simply V/L but

greater depending on the density and distribution of the space charge. Since the photogeneration is field dependent, the enhanced field produces more photoinduced carriers resulting in a larger discharge current. The enhanced field is also responsible for the change in shape of the discharge current. In this case, the electric field modulates the velocity of the carriers as they drift through the material, producing the largest current in the high-field region near the illuminated surface and the lowest current at the substrate. This fatigue effect has also been observed in vitreous Se.[17] The reduced transit time is not as well understood as the other fatigue effects. However, it could be interpreted as a transient space-charge-perturbed effect as described by Weisz *et al.*[14] The reduced transit, then, is caused by both the internal bulk space charge and the increasing electric field felt by the mobile charge as it drifts through the material.

The xerographic $\Delta v(t)/\Delta t_{t=0}$ versus field curve for a 26-μ sample of vitreous As_2Se_3 is shown in Fig. 11. The xerographic quantum efficiency can be obtained directly from this curve as indicated by Eq. (16). The quantum efficiency varies approximately as $E^{0.5}$ for fields greater than 4×10^4 V/cm. This correlates with the electroded quantum efficiency measurements which also showed this field dependence. Below 4×10^4 V/cm, the quantum efficiency falls faster than $E^{0.5}$. No correlation can be made for these small fields since the signal levels for the electroded measurements were too small to make an accurate measurement.

SUMMARY

The transient photoconductivity in vitreous As_2Se_3 can be characterized simply in terms of a field-dependent quantum efficiency and a distribution of field-dependent mobilities. The mobility of the fastest carriers varies linearly with the applied field with a typical value of 4×10^{-5} cm^2/V sec at a field of 10^5 V/cm. Vitreous As_2Se_3 is also sensitive to red light which produces an enhanced electric field and an increased photoresponse.

ACKNOWLEDGMENTS

The author wishes to express his thanks to M. Tabak, D. Pai, and G. Lucovsky for many enlightening discussions concerning the concept of a distribution of field-dependent mobilities. The author is also indebted to H. Scher, who performed the original calculations for the transient SCLC under field-dependent mobility conditions.

[1] S. R. Ovshinsky, Phys. Rev. Letters **21,** 1450 (1968).
[2] M. D. Tabak and P. J. Warter, Jr., Phys. Rev. **173,** 899 (1968).
[3] D. Pai and S. W. Ing, Phys. Rev. **173,** 729 (1968).
[4] J. L. Hartke, Phys. Rev. **125,** 1177 (1962).
[5] W. E. Spear, Proc. Phys. Soc. (London) **B76,** 826 (1960); **B70,** 699 (1957).
[6] M. D. Tabak, J. Phys. Chem. Solids (to be published).
[7] J. K. Viscakas, E. A. Montrimas, and A. A. Payera, Appl. Opt. Suppl. **3,** 79 (1969).
[8] B. T. Kolmiets and E. A. Lebedev, Fiy. Tekh. Poluprov. **1,** 300 (1967).
[9] J. Schottmiller, M. Tabak, G. Lucovsky, and A. Ward, J. Non-Cryst. Solids **4,** 161 (1970).
[10] C. Kittel, *Introduction to Solid State Physics* (Wiley, New York, 1960), Chap. 18, p. 523.
[11] H. T. Li and P. J. Regensburger, J. Appl. Phys. **34,** 1730 (1963).
[12] A. Many and G. Rakavy, Phys. Rev. **126,** 1980 (1962).
[13] W. Helfrich and P. Mark, Z. Physik **166,** 370 (1962).
[14] S. Z Weisz, A. Cobas, S. Trester, and A. Many, J. Appl. Phys. **39,** 2296 (1968).
[15] R. E. Drews, R. Zallen, and R. C. Keezer, Bull. Am. Phys. Soc. **13,** 454 (1968); R. E. Drews, R. Zallen, R. Emerald, and M. Slade (unpublished).
[16] J. Mort (private communication).
[17] M. E. Scharfe and M. D. Tabak, J. Appl. Phys. **40,** 3230 (1969).